# Hyperoxia exposure arrests alveolarization in neonatal rats via PTEN-induced putative kinase 1-Parkin and Nip3-like protein X-mediated mitophagy disorders

XUEFEI YU, YANLI SUN, QING CAI, XINYI ZHAO, ZIYUN LIU, XINDONG XUE and JIANHUA FU

Department of Pediatrics, Shengjing Hospital of China Medical University, Shenyang, Liaoning 110004, P.R. China

Received June 11, 2020; Accepted August 31, 2020

DOI: 10.3892/ijmm.2020.4766

**Abstract.** Bronchopulmonary dysplasia (BPD), also known as chronic lung disease, is one of the most common respiratory diseases in premature new-born humans. Mitochondria are not only the main source of reactive oxygen species but are also critical for the maintenance of homeostasis and a wide range of biological activities, such as producing energy, buffering cytosolic calcium and regulating signal transduction. However, as a critical quality control method for mitochondria, little is known about the role of mitophagy in BPD. The present study assessed mitochondrial function in hyperoxia-exposed alveolar type II (AT-II) cells of rats during lung development. New-born Sprague-Dawley rats were divided into hyperoxia (85% oxygen) and control (21% oxygen) groups. Histopathological and morphological properties of the lung tissues were assessed at postnatal days 1, 3, 7 and 14. Ultrastructural mitochondrial alteration was observed using transmission electron microscopy and the expression of the mitophagy proteins putative kinase (PINK)1, Parkin and Nip3-like protein X (NIX) in the lung tissues was evaluated using western blotting. Immunofluorescence staining was used to determine the co-localisation of PINK1 and Parkin. Real-time analyses of extracellular acidification rate and oxygen consumption rate were performed using primary AT-II cells to evaluate metabolic changes. Mitochondria in hyperoxia-exposed rat AT-II cells began to show abnormal morphological and physiological features. These changes were accompanied by decreased mitochondrial membrane potential and increased expression levels of PINK1-Parkin and NIX. Increased binding between a mitochondria marker (cytochrome C oxidase subunit IV isoform I) and an autophagy marker (microtubule-associated protein-1 light chain-3B) was observed in primary AT-II cells and was accompanied by decreased mitochondrial metabolic capacity in model rats. Thus, mitophagy mediated by PINK1, Parkin and NIX in AT-II cells occurred in hyperoxia-exposed new-born rats. These findings suggested that the accumulation of dysfunctional mitochondria may be a key factor in the pathogenesis of BPD and result in attenuated alveolar development.

*Correspondence to:* Dr Jianhua Fu, Department of Pediatrics, Shengjing Hospital of China Medical University, 36 Sanhao Street, Shenyang, Liaoning 110004, P.R. China
E-mail: fujh@sj-hospital.org

*Key words:* bronchopulmonary dysplasia, lung development, mitophagy, PINK1-Parkin, Nip3-like protein X

## Introduction

Bronchopulmonary dysplasia (BPD) is one of the most common diseases in preterm infants with a gestational age of <30 weeks or a birth weight of <1,200 g, especially in those requiring oxygen inhalation or mechanical ventilation during treatment (1). The major pathological characteristics of BPD are obstruction of alveolarization and simplification of pulmonary vascular development (2,3). Since its initial description in 1967, advances in the comprehensive management technology for BPD in preterm new-borns have increased the survival rate substantially (4,5); however, BPD still affects ~10,000 neonates each year in the United States (6). Thus, further improvements in developmental outcomes and morbidity reduction of BPD are urgently needed (7). The pathogenesis of BPD is extremely complex and remains unclear (8-10), emphasising the need for an improved understanding of alveolar development under both normal and pathological conditions.

Mitochondrial autophagy (mitophagy) is an important process in mitochondrial quality control (11), involving ubiquitin- and receptor-dependent pathways (12). Cells regulate biosynthetic functions by selectively identifying and eliminating damaged or excess mitochondria (11). Abnormal mitophagy is closely associated with lung diseases, such as COPD and pulmonary fibrosis (13); however, the role of mitophagy in BPD is not well-established.

The classic process of mitophagy is primarily mediated by the phosphatase and tensin homolog-induced putative kinase 1 (PINK1)-Parkin pathway. PINK1 is a serine/threonine protein kinase localised on the outer mitochondrial membrane (14). When the mitochondria are healthy in cells, PINK1 is degraded by proteasomes and maintained at a low level (15). However, upon a decrease in the mitochondrial membrane potential (MMP), PINK1 is not transported into the mitochondria but rather aggregates on the outer membrane and recruits Parkin, an E3 ubiquitin ligase (14). Subsequent binding to p62 and microtubule-associated

protein-1 light chain-3B (LC3B) leads to the engulfment and degradation of mitochondria by autophagosomes (16). Several previously identified mitochondrial receptors, such as Nip3-like protein X (NIX), BCL2/adenovirus E1B 19 kDa protein-interacting protein 3 and FUN14 domain-containing protein 1 (17), are located on the outer mitochondrial membrane and directly recruit LC3B for mitochondrial degradation (18). Mitophagy contributes to stem cell differentiation, aging and other pathological processes, such as neurodegenerative diseases, cancer and metabolic diseases (19); however, little is known about its roles in lung development and BPD. Therefore, the present study aimed to assess the effects of PINK1-Parkin and NIX on rat alveolar type II (AT-II) cells, which play a crucial role in the pathogenesis of BPD (20).

Changes in metabolic activity are closely linked to cell fate decisions and development (21). Mitochondria are involved in various biological activities, such as energy synthesis, reduction-oxidation reactions, calcium signalling, reactive oxygen species generation and macromolecule synthesis (22). Therefore, it was hypothesised that mitochondrial injuries induced by hyperoxia impair normal energy synthesis and to contribute to BPD.

To test this hypothesis, the expression of PINK1-Parkin and NIX was evaluated in an experimental rat model and its association with mitochondrial damage and metabolic changes. The present results may help to clarify the role of mitophagy in lung epithelial cells and demonstrate the critical role of mitophagy in lung developmental disorders.

## Materials and methods

*Model establishment and animal treatment*. In total, eight pregnant Sprague-Dawley rats (300-350 g) were purchased from the Department of Animals, Experimental Centre, Shengjing Hospital of China Medical University. Each pregnant rat was fed independently at 20-26˚C, 12 h light/dark cycle and free to access to food and water. Eighty offspring were born on days 21-23 of pregnancy and were randomly divided into a model group (n=40) and control group (n=40) after birth. Following our previously described methods (23), new-born rats in the model group were exposed to a high oxygen environment ($FiO_2$=0.85) within 12 h after birth, and the control group was exposed to normoxic air ($FiO_2$=0.21). The $CO_2$ concentration was controlled at <0.5% using soda lime, and silica gel was used to remove water vapor from the oxygen tank. The maternal rats were used to feed the new-born rats and were exchanged among cages every 24 h to minimise the effect of differences in nursing ability. The cage was opened for 30 min every day and clean drinking water and food were provided. On postnatal day (P)1, 3, 7 and 14 after modelling, 10 pup rats in each group were anaesthetised using pentobarbital sodium (intraperitoneal injection at the dose of 50 mg/kg) and euthanized by cervical dislocation. Then the chest cavity was opened quickly to dissect the lung tissue. All experimental procedures were reviewed and approved by The Ethics Committee of China Medical University (Shenyang, China).

*Histopathology*. After being resected, the left lung was cut to 0.5 cm thickness sections, fixed with 4% paraformaldehyde at room temperature for 48 h and embedded in paraffin, and the right lung was stored at -80˚C for subsequent experiments. The sections were dehydrated using graded ethyl alcohol solutions (75% ethanol overnight, 95% ethanol for 4 h and 100% ethanol for 2 h), and embedded with paraffin after treatment with xylene. The tissue sections were stained with haematoxylin and eosin (haematoxylin for 5 min, rinsed with PBS for 30 min and eosin for 5 min) at room temperature using an automatic dyeing machine (Leica Autostainer XL). Histopathological changes were observed using a light microscope (Eclipse Ci; Nikon Corporation) at x200 magnification. Each slice was analysed in six random regions. The radial alveolar count (RAC) and alveolar wall thickness were determined to evaluate alveolar development using ImageJ software version 1.80 (National Institutes of Health). These assessments were carried out independently by two pathologists who were blinded to the grouping.

*Transmission electron microscopy*. After treatment, 1 $mm^3$ of fresh lung tissue was fixed in 4% paraformaldehyde and 2.5% glutaraldehyde in 0.1 M phosphate buffer overnight at 4˚C and dehydrated in graded ethyl alcohol solutions (50-90%) at 4˚C, before embedding in acetone for 4 h at room temperature. Ultrathin sections (50-60 nm thickness) were obtained and double-stained with uranyl acetate and lead citrate for 30 min at room temperature. Finally, a transmission electron microscope (JEM-1200EX; Hitachi High-Technologies Corporation) was used to observe lung tissue samples from the model group at P1, 3, 7 and 14 at 100 kV. Under a magnification of x10,000 (for six fields of view at each time point), AT-II cells with peculiar lamellar bodies were identified, and the number and morphological changes of mitochondria were recorded. According to previously described methods (24), mitochondrial size were measured. Mitochondrial fragments that were <1 $\mu m^3$ and not divided (usually round) were identified and the average percentage of mitochondrial fragments in the field of view was counted using mitochondrial fragmentation index (MFI). A random double-blind analysis of the mitochondrial structure in AT-II cells was performed. ImageJ software version 1.80 (National Institutes of Health) was used to analyse images obtained using electron microscopy at different time points.

*Western blotting*. The lung tissue was harvested and homogenised in RIPA lysis buffer with a protease inhibitor (P1045; Beyotime Institute of Biotechnology). The protein concentration was measured using the bicinchoninic acid method and samples were boiled with a loading buffer for protein extraction. In total, 15 $\mu$g/lane samples were loaded onto a 4-20% gel, resolved using SDS-PAGE and subsequently transferred to polyvinylidene fluoride (PVDF) membranes. The membranes were then sealed using 5% skimmed milk for 2 h to block non-specific binding at room temperature. The following primary antibodies were used: PINK1 (1:500; cat. no. BC100494; Novus Biologicals), Parkin (1:100; cat. no. sc-32282; Santa Cruz Biotechnology, Inc.), NIX (1:1,000; cat. no. ab8399, Abcam), Cytochrome C oxidase subunit IV isoform I (COX4) (1:500; cat. no. ab14744; Abcam), LC3B (1:1,000; cat. no. 2775; Cell Signalling Technology, Inc.) and β-actin (1:1,000; cat. no. 60008-1-Ig, ProteinTech Group, Inc.). The PVDF membranes were mixed with primary

antibodies, diluted in 10% skimmed milk in Tris-buffered saline and Tween-20 (TBST), and incubated overnight at 4˚C. The next day, after washing with TBST for three times, the PVDF membranes were incubated with a horseradish peroxidase-conjugated secondary antibody (1:10,000; cat. no. SA00001-1 and SA00001-2, ProteinTech Group, Inc.) at 20˚C for 2 h and washed in TBST. Finally, band density was determined using image capture densitometry (GE Amersham Imager 600; Cyvita) using an Enhanced Chemiluminescence Substrate ECL kit (Santa Cruz Biotechnology, Inc.).

*Mitochondrial separation*. Mitochondrial separation was performed using a tissue mitochondrial isolation kit according to the manufacturer's instructions (cat. no. C3606; Beyotime Institute of Biotechnology). The mitochondrial lysis buffer consisted of 0.25 M sucrose, 10 mM Tris-hydrochloric acid, 3 mM $MgCl_2$, 0.1 mM EDTA and a mixture of phosphatase and protease inhibitors. After homogenising the fresh lung tissue with mitochondrial lysis buffer on ice, the homogenate was centrifuged at 4˚C and 600 x g for 5 min. The supernatant was recovered and centrifuged at 11,000 x g at 4˚C for 10 min. The precipitate was washed in the lysis buffer and centrifuged again at 12,000 x g at 4˚C for 15 min. Finally, the mitochondrial precipitate was recovered and suspended in stock solution for the MMP assay.

*Primary AT-II cell isolation*. AT-II cells of new-born rats were isolated on postnatal days 1, 3, 7 and 14. Briefly, lung tissues of new-born rats were perfused with normal saline, cut using scissors and digested with 0.25% trypsin-EDTA (cat. no. 25200056; Gibco; Thermo Fisher Scientific, Inc.) at 37˚C. After 30 min, digestion was terminated and samples were filtered through 60 and 200-$\mu$m filters. The cell pellet obtained after centrifugation at 200 x g at 20˚C for 5 min and was resuspended in 0.1% collagenase I at 37˚C for digestion (cat. no. 17100017; Gibco; Thermo Fisher Scientific, Inc.) The cells were harvested by centrifugation at 200 x g at 20˚C for 5 min, resuspended in Dulbecco's modified Eagle's medium (DMEM) (Corning, Inc.) containing 1% penicillin streptomycin double antibody and 10% fetal bovine serum (10099141; Gibco; Thermo Fisher Scientific, Inc.) and incubated. The culture dish was replaced every 30 min for a total of six times to remove fibroblasts and unattached cells. Finally, an IgG-coated dish was used for differential attachment to remove foreign cells, such as fibroblasts and macrophages. After 12 h, the cells were collected for subsequent experiments.

*MMP assay*. The 5,5',6,6'-tetrachloro-1,1',3,3'-tetraethyl-benzimidazole carbon iodide (JC-1) fluorescent probe (cat. no. C2006; Beyotime Institute of Biotechnology) was used to detect MMP ($mt\Delta\Psi$). In brief, the medium in the six-well plate was discarded and 0.5 mM JC-1 staining working solution was added to primary AT-II cells for 15 min, followed by incubation in the dark environment at 37˚C for 20 min. After washing three times with DMEM (10-013-CV, Corning, Inc.), the $mt\Delta\Psi$ value for each sample was determined as the ratio of the red fluorescence intensity to the green fluorescence intensity. In normal cells, mitochondria have a higher membrane potential, which can cause JC-1 to form orange-red fluorescent J-aggregates outside the mitochondrial membrane (25). In mitochondrial-damaged cells, sensor dyes appear as green fluorescent monomers. Live cells were observed using 80x fluorescent objective. The objective was connected to the Photon Technologies Dual Emission system (LSM880; Zeiss AG) and the excitation wavelength was set to 490 and 525 nm. The fluorescence was emitted and collected separately using Zen Imaging Software3.0. Data are shown as ratios (F590/F530). A decrease in the red (F590)/green (F530) fluorescence intensity ratio indicated a loss of MMP.

*Immunofluorescence double staining*. The extracted primary AT-II cells were plated at 200,000 cells/ml for subsequent detection. The plated cells were washed with PBS and fixed with 4% paraformaldehyde at 4˚C for 30 min. Primary antibodies were added, including antibodies against LC3B (1:200; cat. no. 2775; anti-rabbit, Cell Signalling Technology, Inc.) and COX4 (1:100; cat. no. ab14744; anti-mouse, Abcam), and incubated overnight at 4˚C. After washing with PBS, donkey anti-rabbit IgG H&L (Alexa Fluor® 594; cat. no. ab150076, Abcam) and donkey anti-mouse IgG H&L (Alexa Fluor® 488; cat. no. ab150105; Abcam) were added, incubated for 2 h at room temperature, and counterstained with DAPI for 5 min at room temperature. Similarly, tissue paraffin sections were dehydrated using graded ethanol (75% overnight, 95% for 4 h and 100% for 2 h) and subjected to fluorescent double staining. Primary antibodies against PINK1 (1:100; cat. no. BC100494; anti-rabbit; Novus Biologicals) and Parkin (1:100; cat. no. sc-32282; anti-mouse; Santa Cruz Biotechnology, Inc.) were applied at 4˚C overnight. After washing with PBS, a secondary antibody labelled with fluorescein isothiocyanate (Alexa Fluor® 594; cat. no. ab150076, and Alexa Fluor® 488; cat. no. ab150105; both Abcam) was added and incubated for 2 h and counterstained with DAPI for 5 min, both at room temperature. After observation at x400 magnification using a two-photon confocal microscope (LSM880; Zeiss AG), 3-dimensional reconstruction was performed using ImageJ software1.80, which was also used to analyse the changes in fluorescence intensity changes.

*Seahorse XF energy analysis*. The oxygen consumption rate (OCR) and extracellular acidification rate (ECAR) were measured using the Seahorse XFe96 Flux Analyzer (Agilent Technologies, Inc.). According to methods suggested by the manufacturer, rat primary AT-II cells were extracted on P3, 7 and 14. Cells were seeded on XF96 cell plates (Agilent Technologies, Inc.) at a density of 20,000 cells/well. On-board testing was performed 12 h after seeding. The original medium in the cell plate was discarded and replaced with serum-free bicarbonate-containing analysis medium (10 mM glucose, 2 mM glutamine and 1 mM ammonium pyruvate). For the mitochondrial stress test, based on pilot experiments with the oxidative phosphorylation uncoupling agent Trifluoromethoxy carbonylcyanide phenylhydrazone (FCCP) at four concentrations of 0.5, 1, 1.5 and 2 mM, the optimal concentration was identified as 2 mM for the subsequent detection in AT-II cells. Oligomycin, Rotentone and Antimycin A were used at the concentrations specified in the manufacturer's instructions. No glucose was added in the first stage to detect basal respiration. In the second stage, oligomycin was added to detect the ATP-related metabolic capacity of mitochondria. In the

third stage, the uncoupling agent FCCP was added to detect the maximum mitochondrial pressure. Finally, rotenone and antimycin A were added to detect the non-mitochondrial oxygen consumption. Similarly, metabolic regulators, such as glucose, oligomycin and 2-deoxyglucose (2-DG), were used for glycolytic stress according to the method described by the manufacturer. No glucose was added and extracellular acidification was tested in the first stage. In the second stage, glycolysis was detected after the addition of glucose. In the third stage, oligomycin was added to detect the maximum storage capacity of glycolysis. In the fourth stage, 2-DG was added to detect the residual capacity of glycolysis. Ten biological replicates were established for each group.

*Statistical analysis*. Data analysis was performed using GraphPad Prism version 8.0 (GraphPad Software). Parameters were compared between groups using the unpaired Student's t-tests at each time point and no multiple comparisons were made across timepoints or within a timepoint. Correlation analysis was performed using Pearson's tests. All data are expressed as means ± standard error of the mean. n represents the number of animals in each group or the number of independent experiments. $P<0.05$ was considered to indicate a statistically significant difference.

## Results

*Hyperoxia exposure leads to delayed alveolarization*. New-born lung tissues rats were collected at P1, 3, 7 and 14 after exposure to normoxic or hyperoxic conditions and were evaluated with respect to alveolar development. In the two groups, the number of alveoli and capillaries increased gradually. With a decrease in the alveolar cavity diameter and an increase in the alveolar ridge structure, the thickness of the alveolar septum gradually decreased. Compared with the control group (n=10), the model group (n=10) showed a widened alveolar septum, oedema and inflammatory cell infiltration in some fields at P3 (Fig. 1A). There was no statistically significant difference in alveolar RAC values between the control and model groups at P1 and P3 (both $P>0.05$). Similarly, there was no significant difference in alveolar wall thickness between the groups at P1 and P3 (both $P>0.05$). However, from P7, the alveolar diameter in the model group was larger compared with that in the control group, and the alveolar ridge structure was reduced and blunt. The RAC was lower in the model group ($P<0.01$; Fig. 1B), whereas the thickness of the lung septum was higher ($P<0.01$; Fig. 1C) in the model group compared with the control group. These results showed that the model group had alveolar growth delay at P7 and P14.

*Hyperoxia exposure leads to mitochondrial morphological disorders in AT-II cells*. The mitochondria of AT-II cells in each group were observed using transmission electron microscopy and the ultrastructures were compared. In the control group, there were compact mitochondria, abundant lipid lamellar bodies and a normal basic cell substructure. The volume of the mitochondria gradually increased and the crista gradually became denser in the control group. The mitochondrial structure was disrupted in the model group as of P3. This was manifested as mitochondrial swelling and fracture, destruction of the mitochondrial double membrane structure, mitochondrial cristae disappeared, and the mitochondria became longer and increasingly divided. Peculiar lamellar corpuscle structural damage. After oxygen exposure, mitochondria were ruptured and mitophagosomes wrapped in autophagosome membranes were observed in the zoomed-in images (Fig. 2A). At P3, the MFI was significantly increased ($P<0.05$), but swelling also increased, and the average mitochondrial area did not differ from that in the control group ($P>0.05$). However, from P7, the MFI and mitophagosomes in the model group were significantly increased ($P<0.01$) and the average mitochondria area was significantly lower compared with that in the control group ($P<0.01$) (Fig. 2A-D). In summary, mitochondrial damage in AT-II cells of the model group increased gradually over time, with increases in swelling and fragmentation becoming more obvious over time.

*Hyperoxia exposure leads to decreased MMP in AT-II cells*. A decrease in MMP is a sensitive signal of mitochondrial damage and autophagy activation (26). Accordingly, MMP was measured in primary AT-II cells (n=6) using the fluorescence intensity (Fig. 3A) and ratio of JC-1 polymer levels (red)/JC-1 monomer levels (green) to evaluate mitochondrial function damage in the model group at each time point. At P3, the mtΔΨ was 0.605 in the model group, while the mtΔΨ ratio was 0.937 in the control ($P<0.05$). And the mtΔΨ ratio decreased to 0.564 at P7 ($P<0.05$) and 0.437 at P14 ($P<0.01$), while the mtΔΨ fluorescence intensity ratio was 1.004 in the control group at P7 and 0.876 at P14 (Fig. 3B). The mtΔΨ ratio of the model group was lower compared with that of the control group in AT-II cells. The membrane potential of mitochondria extracted from the lung tissues was also detected using JC-1 staining within 30 min and measured fluorescence intensity using a microplate reader. The mtΔΨ was 1.280 in the control and 0.994 in the model group at P3, the difference from the control group was statistically significant ($P<0.05$). The mtΔΨ in the model group was 0.742 times less compared with the control group at P7 and 0.478 times less compared with the control group at P14 ($P<0.01$; Fig. 3C and D). These results showed that the MMP in the model group decreased under hyperoxia exposure.

*Increase in mitophagy protein expression in hyperoxia-exposed lung tissues of rats with simple lung structures*. PINK1-Parkin double staining was evaluated in lung tissue sections to assess the ability of PINK1 to recruit Parkin (Fig. 4A). The two proteins were distributed in the cytoplasm of lung cells. The co-localisation of PINK1 and Parkin fluorescence was lower at P3 and higher at P7 and P14 in the model group compared with the control group. Next, the protein levels of PINK1 and Parkin in lung tissues were investigated using western blotting (Fig. 4B-E). Compared with that in the control group, the expression of PINK1 in the model group was significantly elevated at P7 and P14 ($P<0.05$ and $P<0.01$, respectively; Fig. 4C). Consistently, the expression level of Parkin in the model group was not different at P1 or P3 compared with that in the control group; however, a significant difference was observed at P7 and P14 ($P<0.01$ and $P<0.05$, respectively; Fig. 4E). The transformation of LC3B

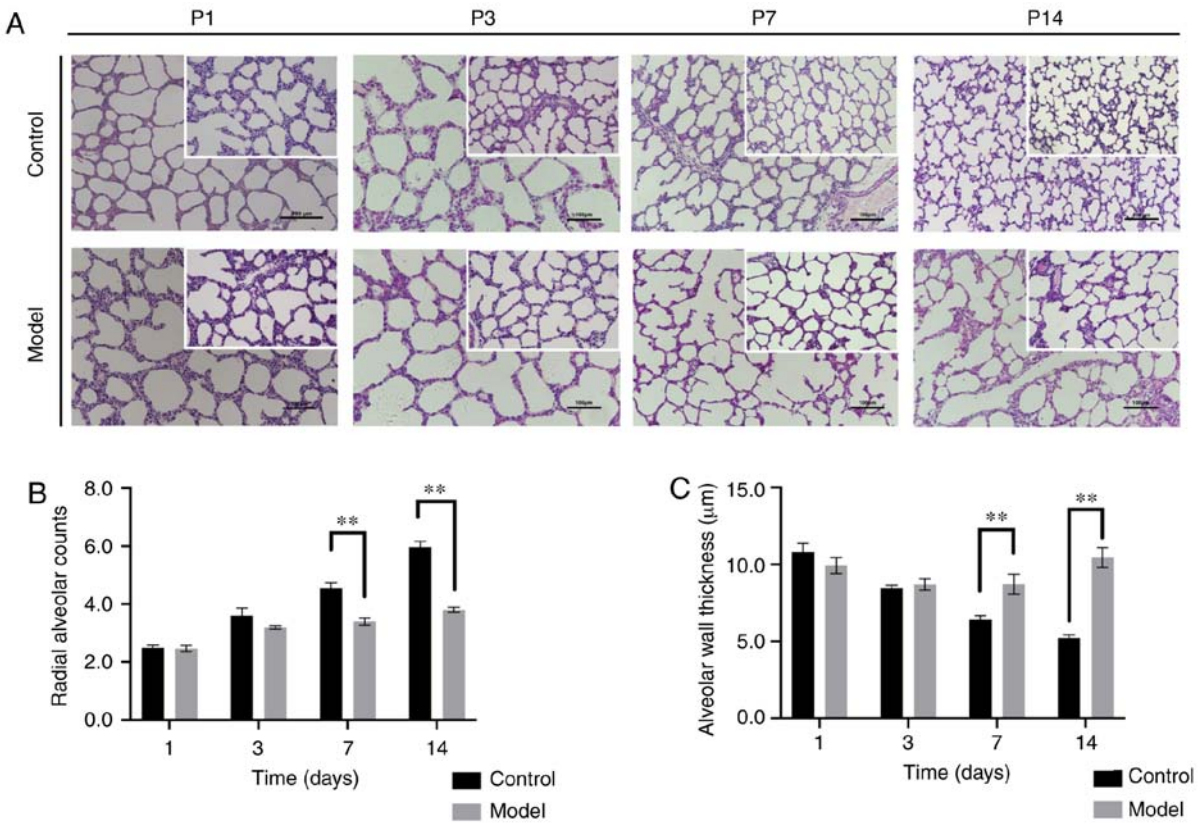


Figure 1. Hyperoxia exposure leads to a delay of alveolarization. (A) Haematoxylin and eosin staining of the lung tissues of new-born rats at P1, 3, 7 and 14 after birth was observed using microscopy (x200 magnification; scale bar, 100 $\mu$m). Changes in lung morphology were quantified using (B) radial alveolar counts and (C) alveolar wall thickness. The data are expressed as mean ± SEM. $^{**}$P<0.01 vs. control. P, postnatal day.

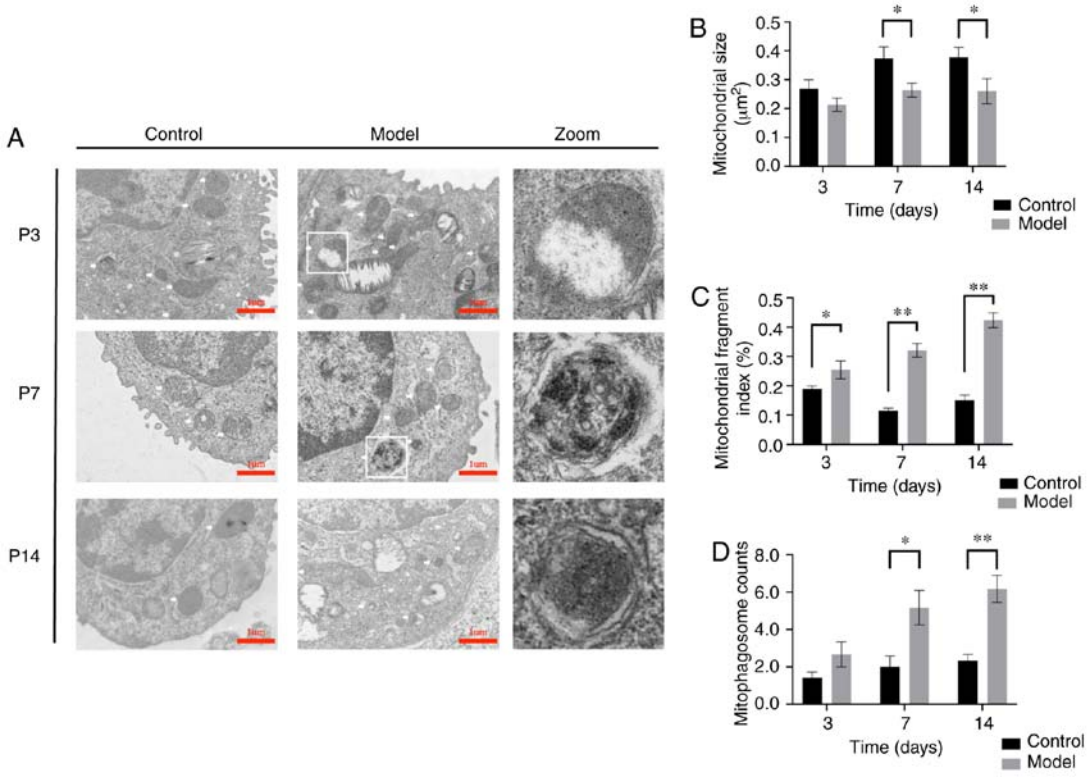


Figure 2. Hyperoxia exposure leads to mitochondrial morphological changes in AT-II cells. (A) Structural changes of mitochondria (x10,000 magnification; scale bar, 1 $\mu$m) were observed using transmission electron microscopy, images showes mitochondria morphological changes in the cells (white arrow). (B) Quantitative measurement of AT-II cell mitochondrial size in each group (n=30/area). (C) Mitochondrial fragmentation index; comparison of the mitochondrial area at different time points. (D) Quantitative measurement of AT-II cell mitophagosome per cell in each group. The data are expressed as mean ± SEM. $^{*}$P<0.05, $^{**}$P<0.01 vs. control. AT-II, alveolar type II cells; P, postnatal day.

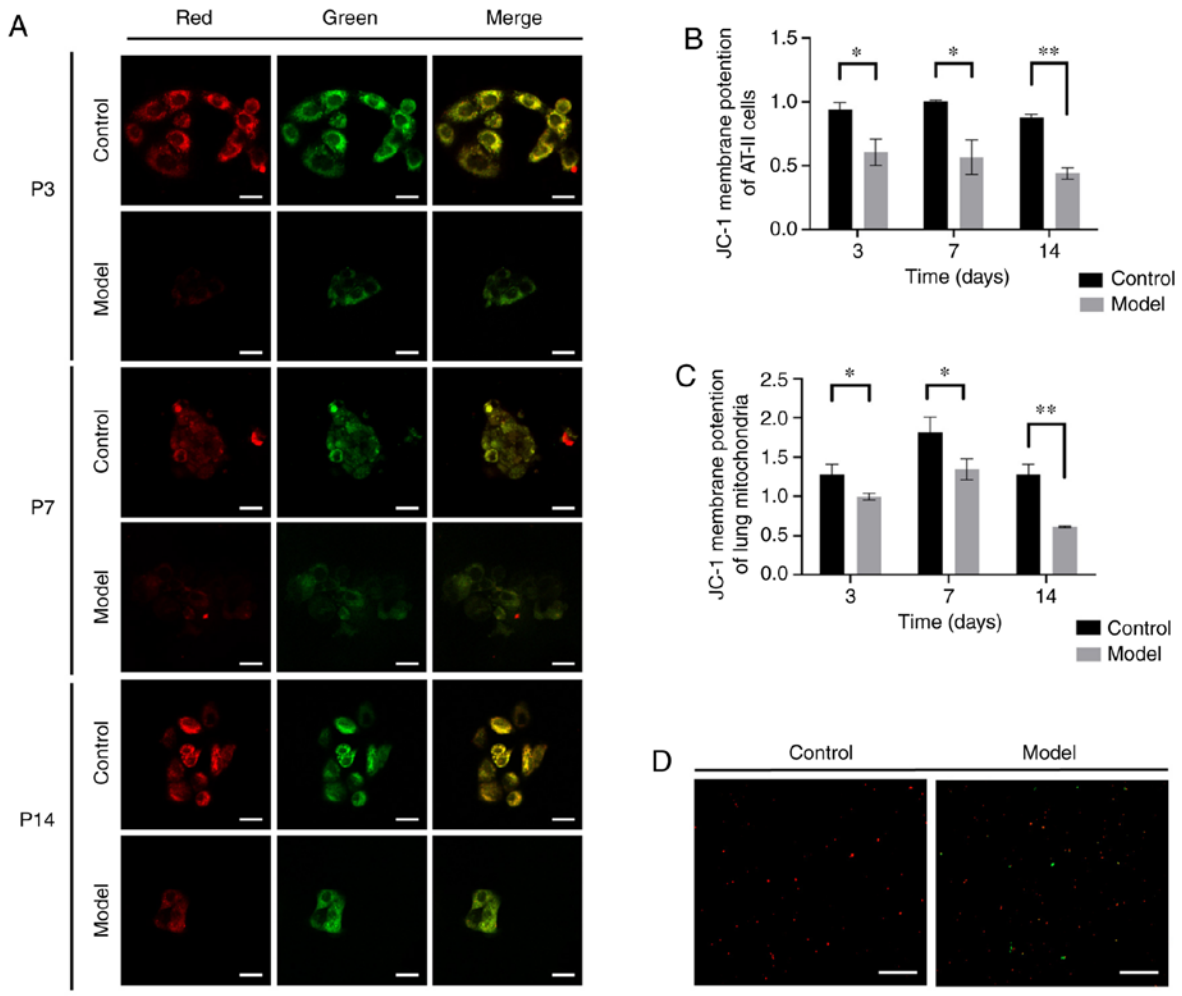


Figure 3. Measurement of MMP depolarisation using JC-1 probes. (A) Representative immunostaining of primary AT-II cells from control and model groups assessed using JC-1 staining (x800 magnification; scale bar, 25 $\mu$m). JC-1 polymer is shown in red and JC-1 monomer is shown in green. (B) Fluorescence intensities (ratio of JC-1 red/green) in primary AT-II cells at P3, 7 and 14. (C) Fluorescence intensities (ratio of JC-1 red/green) in lung tissue mitochondria at P3, 7 and 14. (D) Representative immunostaining of JC-1 staining in lung tissues in the two groups at P14 (x800 magnification; scale bar, 25 $\mu$m). The data are expressed as mean ± SEM, n=3. $^{*}$P<0.05, $^{**}$P<0.01 vs. control. AT-II, alveolar type II cells; P, postnatal day; MMP, mitochondrial membrane potential.

from LC3BI (the free form) to LC3BII (the conjugated form of phosphatidyl ethanolamine) is an important process in the formation of autophagosomes (27). LC3BII/I expression levels in the model group were significantly elevated compared with the control group at P1, 3, 4 and 7 (P<0.05 or P<0.01; Fig. 4D). These results suggested that mitophagy occurred more frequently in the model group compared with the control group.

*Mitophagy in AT-II cells increases in hyperoxia-exposed lung tissues of rats with simple lung structures*. After clarifying the overall protein expression levels of PINK1 and Parkin during lung development, the co-localisation between the mitochondrial marker protein COX4 and autophagy marker protein LC3B was evaluated in primary AT-II cells in the postnatal period. A hallmark of the mitophagy process is the co-localisation of mitochondria with autophagosomes for elimination (28). Immunofluorescence revealed higher LC3B protein levels in the model group compared with in the control group, reaching a peak at P7 (Fig. 5A and B). In addition, the COX4 expression level was no significantly different between the two groups (P>0.05) at each time point (Fig. 5C and E), but the NIX expression level was higher in the model group compared with in the control group (P<0.05) from P1 (Fig. 5C and D) and it was negatively correlated with radial alveolar counts (r=-0.32, P<0.05) (Fig. 5F). These results indicated that NIX mediated mitophagy also occurred more frequently in the model group compared with in the control group and participated in the pathological process of BPD.

*Hyperoxia leads to metabolic changes in primary AT-II cells of model rats with simple lung structures*. Real-time analyses of ECAR and OCR were performed with primary AT-II cells using the Seahorse XF96 metabolic extracellular flux analyser. Anaerobic metabolism levels were evaluated. At P7, non-glycolytic acidification, glycolytic capacity and the glycolytic reserve were significantly lower in the model group compared with in the control group (P<0.05 or P<0.01) (Fig. 6A and B). There were no significant differences in the cellular glycolysis levels between groups under basic conditions. However, as for the mitochondrial pressure and aerobic metabolism levels, the basal respiration capacity, ATP generation capacity (both P<0.05) and remaining respiration capacity of the model group (P<0.01) were higher at P3 in the model group compared with

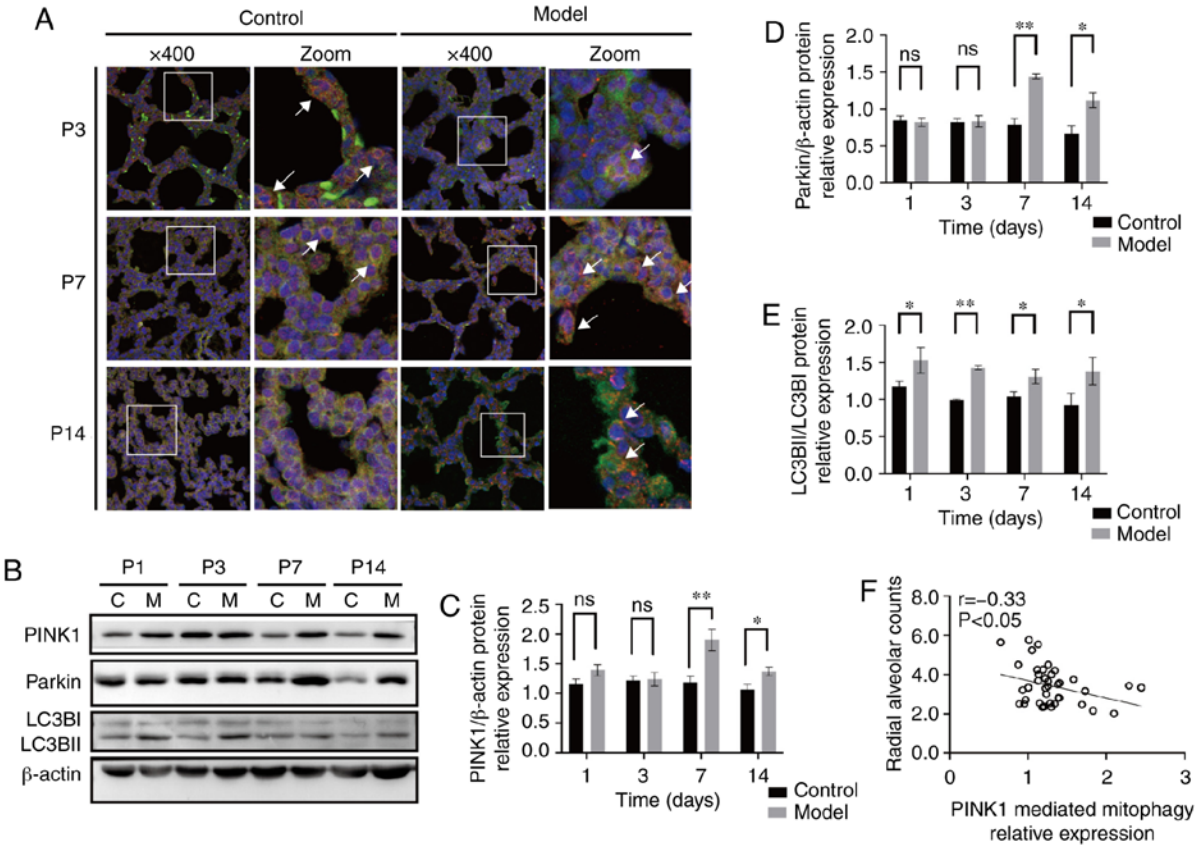


Figure 4. Expression changes of PINK1 and Parkin in the lung tissues of rats with bronchopulmonary dysplasia. (A) Representative immunostaining of lung sections from the two groups using anti-PINK1 (red) and anti-Parkin (green) antibodies. Yellow puncta denote co-localisation. Magnification, x400. (B) Western blot analyses of PINK1, Parkin and LC3BI/LC3BII in the lungs in the C group and M group at P1, 3, 7 and 14. (C) Density analyses of PINK1. (D) Density analyses of Parkin. (E) Density analyses of LC3BII/LC3BI. Blots were stripped and reblotted using an anti-β-actin antibody as a loading control. (F) Correlation analyses between radial alveolar counts and PINK1 mediated mitophagy relative expression in rat lungs. PINK1 mediated mitophagy was negatively correlated with the alveolar development index (r=-0.33; P<0.05). The data are expressed as mean ± SEM from at least six different experiments. $^{*}$P<0.05, $^{**}$P<0.01 vs. control. P, postnatal day; PINK1, putative kinase 1; C, control; M, model; ns, not significant; LC3B, microtubule-associated protein-1 light chain-3B.

in the control group. At P7, the maximal respiration and spare respiratory capacity were significantly lower in the model group compared with in the control group (P<0.01) and the results showed no difference at P14 (Fig. 6C and D). These results suggested that there was a change in the metabolic capacity after hyperoxia exposure at P3 and P7.

## Discussion

Supplemental oxygen is the most common therapeutic agent used in neonatal treatment worldwide; however, prolonged exposure to high oxygen alters the development of lung tissues and vascular beds, resulting in BPD in preterm infants (29-31). The overall incidence of BPD in infants born at <28 weeks of gestational age is estimated to be 48-68% according to a study performed at the National Institute of Child Health and Human Development Neonatal Research Network (3). BPD is a multifactorial disease; however, one of its major risk factors is premature exposure of the lungs to a hyperoxic environment that leads to the production of superfluous reactive oxygen species (32). Mitochondria are not only the main source of reactive oxygen species but are also critical for the maintenance of homeostasis and a wide range of biological activities, such as producing energy, buffering cytosolic calcium and regulating signal transduction (33). However, the role of mitophagy in BPD is not well-established. Therefore, it was hypothesised that mitochondrial injuries induced by hyperoxia impair normal biological mitophagy functions, thereby leading to the onset of BPD.

To adapt to extrauterine life after birth and for postnatal energy production during lung development, various lung cell types undergo mitochondrial morphological changes, including changes to volume density, size, number and distribution (34). In the present study, oxygen exposure in new-born rats resulted in a relatively large alveolar cavity, irregularly spaced lungs and a decreased radial alveolar count. In addition to alveolar morphological changes, the MMP in the model group decreased at the early stage of hyperoxia exposure. The volume of the mitochondria gradually increased and the crista gradually became denser in the control group, whereas in the model group, the level of mitochondrial disruption and fragments increased over time. This suggests that hyperoxia exposure leads to delayed alveolarization and mitochondrial morphological disorders in AT-II cells.

As a major mechanism of mitochondria quality control, mitophagy is responsible for the degradation and recycling of damaged mitochondria (35). PINK1 can recruit Parkin and the two proteins act synergistically to mark damaged mitochondria for clearance by the activation of downstream mitophagy (36). However, the involvement of mitophagy

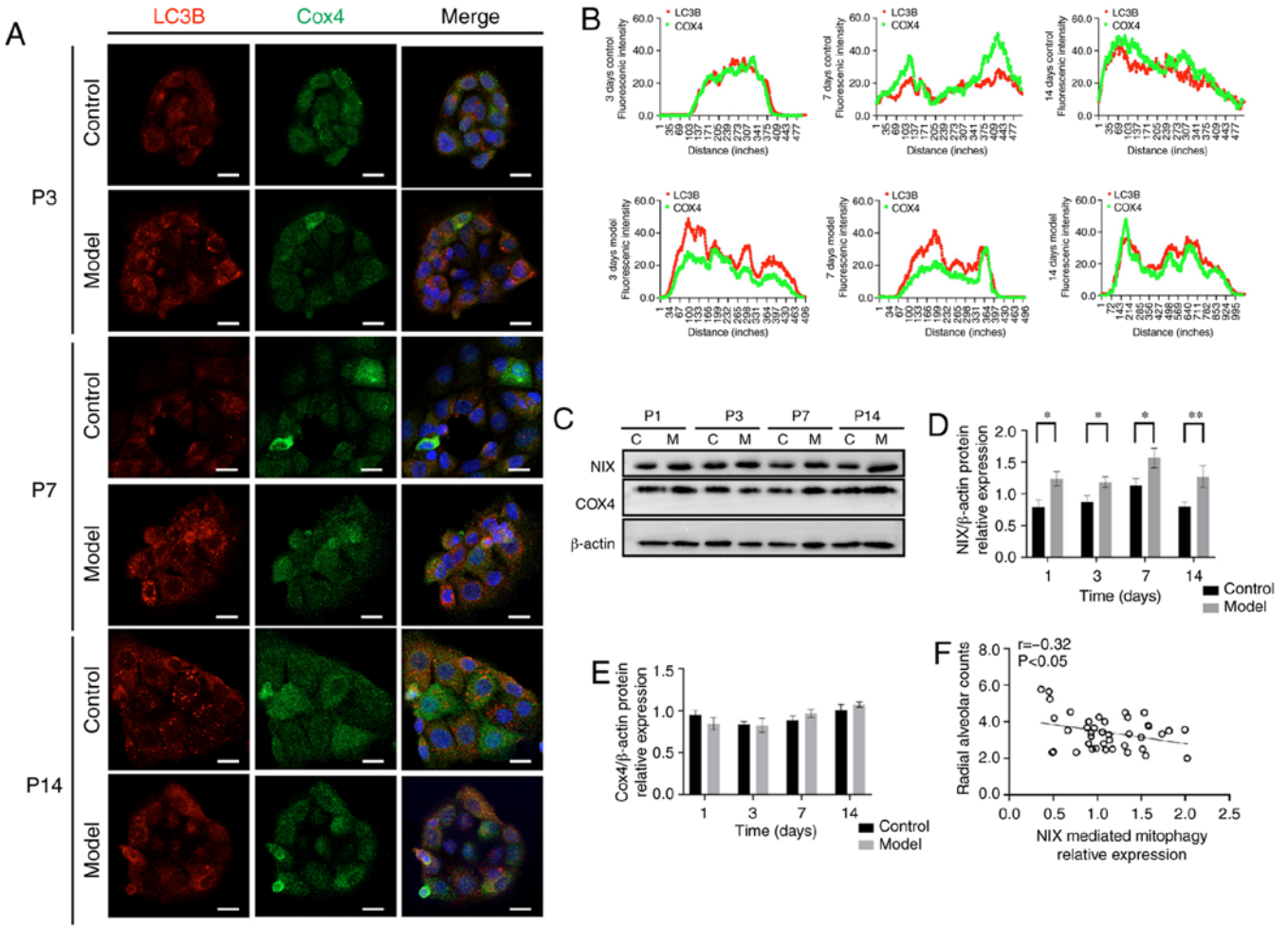


Figure 5. Changes in mitophagy levels in AT-II cells of rats with bronchopulmonary dysplasia. (A) Representative immunostaining of AT-II cell fluorescence double staining (x800 magnification; scale bar, 25 $\mu$m). Green represents the mitochondria marker (COX4), red represents autophagosome marker (LC3B) and double staining is shown in yellow. (B) Line scan data of fluorescence intensity in the corresponding images to show the degree of co-localisation of COX4 and LC3B using ImageJ software1.80. (C) Western blot analyses of NIX and COX4 in the lungs in the C group and M group. Density analyses of (D) NIX and (E) COX4. Blots were stripped and reblotted using an anti-β-actin antibody as a loading control. (F) Correlation analyses between radial alveolar counts and NIX mediated mitophagy relative expression in the rat lungs. NIX-mediated mitophagy was negatively correlated with alveolar development index (r=-0.32; P<0.05). Data represent at least six independent experiments and are presented as mean ± SEM. $^{*}$P<0.05, $^{**}$P<0.01 vs. control. AT-II, alveolar type II cells; COX4, cytochrome C oxidase subunit IV isoform I; LC3B, microtubule-associated protein-1 light chain-3B; NIX, Nip3-like protein X; C, control; M, model.

in chronic lung disease is controversial. Disruptions in mitophagy caused by PINK1 deficiency were reported to promote the occurrence of pulmonary fibrosis (37). However, an increase in PINK1 expression has also been observed and the disturbance of mitophagy appears to be pathogenic in chronic obstructive pulmonary disease (38,39). In the present study, the levels of PINK1 and Parkin were not significantly higher on days P1 and P3, but were higher on days P7 and P14, in the model group compared with those in the control group. Correlation analysis between RAC and PINK1-Parkin mediated mitophagy revealed a negative correlation. Fluorescence double staining indicated the co-localisation of PINK1 and Parkin was also higher in the model group compared with that in the control group, and the combination was most significant at P7. Our previous study showed that the use of rapamycin, a classic autophagy inducer, can improve alveolar morphology development in a rat-based BPD model (40), as used in the present study. Mitophagy is a type of macro-autophagy; however, traditional autophagic inhibition does not prevent PINK1-Parkin-mediated mitophagy and the inhibition of Parkin can affect mitochondrial clearance (41), which suggests that insufficient mitophagy mediated by PINK1-Parkin in the early stage and the recruitment capacity does not continue to increase linearly as the duration of hyperoxia exposure increases. It was therefore hypothesised that PINK1-Parkin-mediated mitophagy disorders may participate in the pathological process of BPD.

NIX is involved in the differentiation and development of stem cells, such as the development of the nervous system (18), retinal ganglion cells (42) and macrophages (42,43). Additionally, NIX may be a substrate of PARK2 in the PINK1-Parkin pathway (44). In the present study, the NIX expression level was higher in the model group compared with that in the control group at all timepoints. Moreover, the negative correlation between RAC and NIX-mediated mitophagy suggests that NIX may also participate in the pathological process of BPD.

Mitochondrial and metabolic changes in cells and their regulatory processes in BPD have been a focus of recent research (21,45). Unlike other cells, AT-II cells tend to use

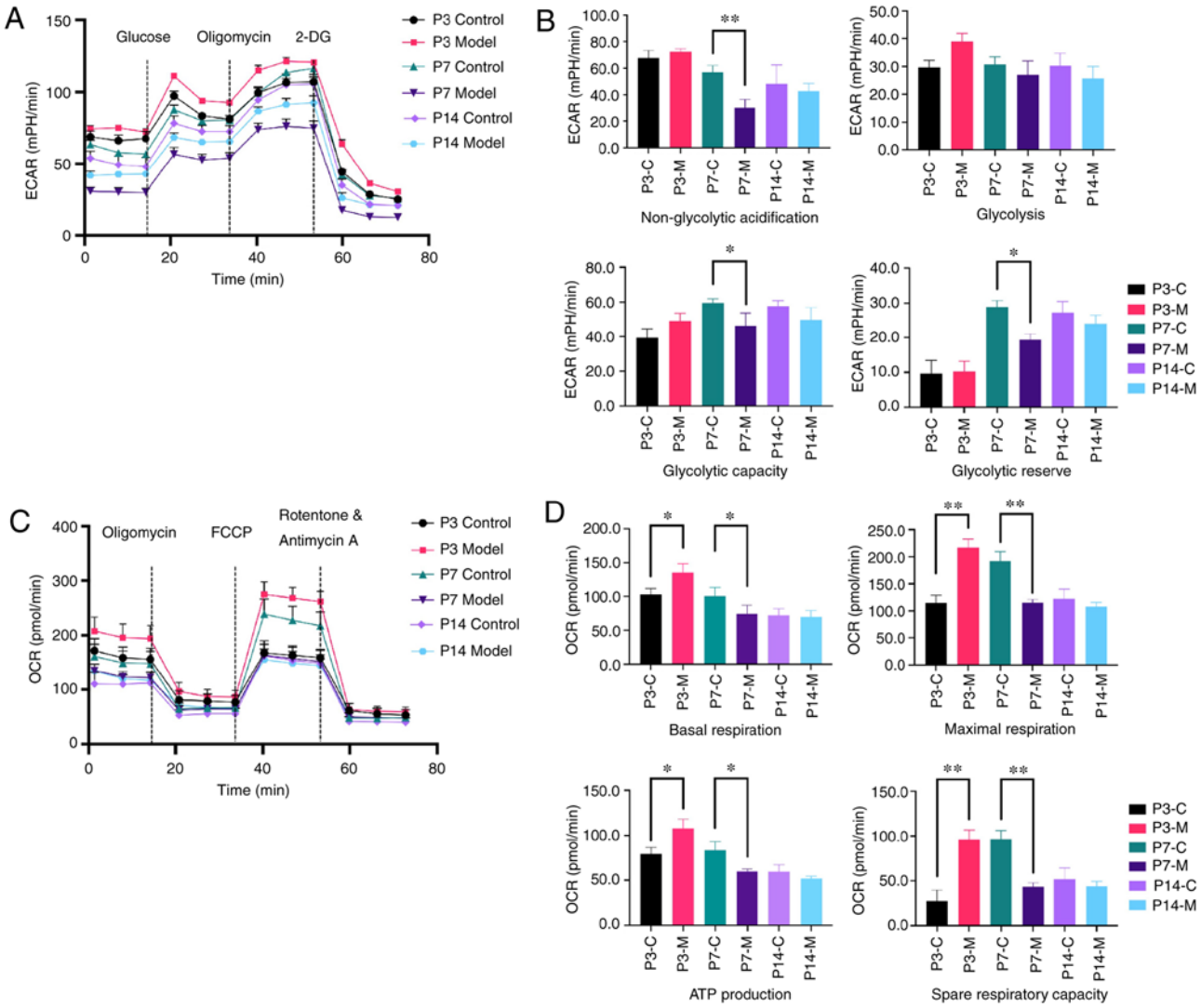


Figure 6. Changes in metabolic activity in primitive AT-II cells. Seahorse XF96 was used to test the ECAR and OCR in primary AT-II cells using real-time analysis. (A) Representative graph of the ECAR output of AT-II cells and responses to glucose, oligomycin and 2-DG. (B) Anaerobic metabolism levels were evaluated. (C) Representative graph of the OCR output of AT-II cells and responses to oligomycin, FCCP and rotenone/antimycin A. (D) Mitochondrial pressure and aerobic metabolism levels were tested. The assay was run in one plate with 10 replicates and data are presented as mean ± SEM. $^{*}$P<0.05, $^{**}$P<0.01 vs. control. ECAR, extracellular acidification rate; OCR, oxygen consumption rate; AT-II, alveolar type II cells; FCCP, trifluoromethoxy carbonylcyanide phenylhydrazone; P, postnatal day. C, control; M, model; 2-DG, 2-deoxyglucose.

lactic acid as a substrate for mitochondrial respiration (46). Accordingly, premature oxygen exposure may change the glucose-oxygen metabolism balance and affect the development of AT-II cells. The present study the tested mitochondrial metabolic function of these cells to confirm the increase of mitochondrial damage in hyperoxia-exposed neonatal rats. After 3 days, the mitochondrial pressure and aerobic function in the model group were higher and, after 7 days, the mitochondrial pressure and glycolytic function were lower compared with those in the control group. This indicated that the model group exhibited metabolic changes. These findings demonstrated that metabolic changes are only significant at the early phase before BPD is established, suggesting that they may be a cause of mitophagy disorders rather than a direct contributor to alveolar morphological changes. Ratner *et al* (47) exposed neonatal rats to 75% $O_2$ for 72 h, followed by recovery in room air for 3 weeks or 2 weeks of hyperoxia exposure. The study showed that mitochondrial OCR and ATP production decreased in the lung tissue, suggesting that the inhibition of mitochondrial oxidative phosphorylation (OXPHOS) is associated with bronchopulmonary developmental arrest. Das (48) conducted metabolic tests *in vitro* in hyperoxia-induced MLE-12 cells. Das observed that the glycolytic reserve capacity and glycolytic residual capacity were reduced and the OXPHOS ability was impaired. Simon *et al* (49) demonstrated that glycolytic capacity exhibits a compensatory increase in AT-II cells at 95% $O_2$; however, this was not accompanied by altered activities of critical mitochondrial (cytochrome oxidase) or glycolytic (pyruvate kinase and phosphofructokinase) enzymes. The present results define the metabolic changes in the early stages of BPD. It is worth noting that mitophagy is also closely related to the metabolic transformation (50). McCoy *et al* (51) reported that the recruitment of Parkin requires hexokinase activity and Liu *et al* reported that Parkin can regulate pyruvate kinase M2 (52). The present study did not fully explore the mechanism underlying the regulation

of metabolic targets, therefore this should be a focus of future research.

In conclusion, the present study demonstrated that there was mitochondrial structural damage and decreased MMP, as well as elevated levels of PINK1-Parkin and the mitophagy receptor protein NIX, in rat AT-II cells under hyperoxia, and that the mitochondrial damage gradually increased over time. Corresponding changes in mitochondrial metabolic capacity were also observed. Thus, the accumulation of dysfunctional mitochondria and abnormalities in mitophagy in the lung tissues may be key factors in the pathogenesis of BPD and could serve as therapeutic targets.

**Acknowledgements**

The authors would like to thank the technical support by Professor Dongyan Liu from Department of Immunology, Shengjing Hospital of China Medical University and the technical support in immunofluorescence double staining provided by Mr. Ziying Li, Miss Yue Zhan and Mr. Jianing Miao from the Department of Research and Development Centre, Shengjing Hospital of China Medical University.

**Funding**

This study was supported by grants from The National Natural Science Foundation of China (grant no. 81571479) and The 345 Talent Project of the Shengjing Hospital (grant no. M0428).

**Availability of data and materials**

The datasets used and/or analyzed during the current study are available from the corresponding author on reasonable request.

**Authors' contributions**

XY and JF conceived and designed the study. XY, YS, QC, XZ and ZL performed the experiments. XY, YS and XX analysed the data and JF reviewed the data. XY wrote the manuscript. All authors read and approved the final manuscript.

**Ethics approval and consent to participate**

The present study was approved by The Ethics Committee of China Medical University (Shenyang, China).

**Patient consent for publication**

Not applicable.

**Competing interests**

The authors declare that they have no competing interests.

**References**

1. Abman SH, Bancalari E and Jobe A: The evolution of bronchopulmonary dysplasia after 50 years. Am J Respir Crit Care Med 195: 421-424, 2017.
2. Surate Solaligue DE, Rodriguez-Castillo JA, Ahlbrecht K and Morty RE: Recent advances in our understanding of the mechanisms of late lung development and bronchopulmonary dysplasia. Am J Physiol Lung Cell Mol Physiol 313: L1101-L1153, 2017.
3. Stoll BJ, Hansen NI, Bell EF, Shankaran S, Laptook AR, Walsh MC, Hale EC, Newman NS, Schibler K, Carlo WA, *et al*: Neonatal outcomes of extremely preterm infants from the NICHD neonatal research network. Pediatrics 126: 443-456, 2010.
4. García-Muñoz Rodrigo F, Losada Martínez A, Elorza Fernández MD, Moreno Hernando J, Figueras Aloy J and Vento Torres M: The burden of respiratory disease in very-low-birth-weight infants: Changes in perinatal care and outcomes in a decade in Spain. Neonatology 112: 30-39, 2017.
5. Dumpa V and Bhandari V: Surfactant, steroids and non-invasive ventilation in the prevention of BPD. Semin Perinatol 42: 444-452, 2018.
6. Kalikkot Thekkeveedu R, Guaman MC and Shivanna B: Bronchopulmonary dysplasia: A review of pathogenesis and pathophysiology. Respir Med 132: 170-177, 2017.
7. Jobe AH and Abman SH: Bronchopulmonary dysplasia: A continuum of lung disease from the fetus to the adult. Am J Respir Crit Care Med 200: 659-660, 2019.
8. Chen Y, Chang L, Li W, Rong Z, Liu W, Shan R and Pan R: Thioredoxin protects fetal type II epithelial cells from hyperoxia-induced injury. Pediatr Pulmonol 45: 1192-1200, 2010.
9. McGrath-Morrow SA and Stahl J: Apoptosis in neonatal murine lung exposed to hyperoxia. Am J Respir Cell Mol Biol 25: 150-155, 2001.
10. O'Reilly MA, Staversky RJ, Finkelstein JN and Keng PC: Activation of the G2 cell cycle checkpoint enhances survival of epithelial cells exposed to hyperoxia. Am J Physiol Lung Cell Mol Physiol 284: L368-L375, 2003.
11. Bayne AN and Trempe JF: Mechanisms of PINK1, ubiquitin and Parkin interactions in mitochondrial quality control and beyond. Cell Mol Life Sci 76: 4589-4611, 2019.
12. Wang Y, Liu N and Lu B: Mechanisms and roles of mitophagy in neurodegenerative diseases. CNS Neurosci Ther 25: 859-875, 2019.
13. Sureshbabu A and Bhandari V: Targeting mitochondrial dysfunction in lung diseases: Emphasis on mitophagy. Front Physiol 4: 384, 2013.
14. Meissner C, Lorenz H, Weihofen A, Selkoe DJ and Lemberg MK: The mitochondrial intramembrane protease PARL cleaves human Pink1 to regulate Pink1 trafficking. J Neurochem 117: 856-867, 2011.
15. Nardin A, Schrepfer E and Ziviani E: Counteracting PINK/Parkin deficiency in the activation of mitophagy: A potential therapeutic intervention for Parkinson's disease. Curr Neuropharmacol 14: 250-259, 2016.
16. Liu H, Dai C, Fan Y, Guo B, Ren K, Sun T and Wang W: From autophagy to mitophagy: The roles of P62 in neurodegenerative diseases. J Bioenerg Biomembr 49: 413-422, 2017.
17. Wei H, Liu L and Chen Q: Selective removal of mitochondria via mitophagy: Distinct pathways for different mitochondrial stresses. Biochim Biophys Acta 1853: 2784-2790, 2015.
18. Deczkowska A and Schwartz M: NIX-ing mitochondria: From development to pathology. EMBO J 36: 1650-1652, 2017.
19. Um JH and Yun J: Emerging role of mitophagy in human diseases and physiology. BMB Rep 50: 299-307, 2017.
20. Yee M, Vitiello PF, Roper JM, Staversky RJ, Wright TW, McGrath-Morrow SA, Maniscalco WM, Finkelstein JN and O'Reilly MA: Type II epithelial cells are critical target for hyperoxia-mediated impairment of postnatal lung development. Am J Physiol Lung Cell Mol Physiol 291: L1101-L1111, 2006.
21. Cliff TS and Dalton S: Metabolic switching and cell fate decisions: Implications for pluripotency, reprogramming and development. Curr Opin Genet Dev 46: 44-49, 2017.
22. Aravamudan B, Thompson MA, Pabelick CM and Prakash YS: Mitochondria in lung diseases. Expert Rev Respir Med 7: 631-646, 2013.
23. Hou A, Fu J, Yang H, Zhu Y, Pan Y, Xu S and Xue X: Hyperoxia stimulates the transdifferentiation of type II alveolar epithelial cells in newborn rats. Am J Physiol Lung Cell Mol Physiol 308: L861-L872, 2015.
24. Hara H, Araya J, Ito S, Kobayashi K, Takasaka N, Yoshii Y, Wakui H, Kojima J, Shimizu K, Numata T, *et al*: Mitochondrial fragmentation in cigarette smoke-induced bronchial epithelial cell senescence. Am J Physiol Lung Cell Mol Physiol 305: L737-L746, 2013.

25. Resseguie EA, Brookes PS and O'Reilly MA: SMG-1 kinase attenuates mitochondrial ROS production but not cell respiration deficits during hyperoxia. Exp Lung Res 43: 229-239, 2017.
26. Song SB, Jang SY, Kang HT, Wei B, Jeoun UW, Yoon GS and Hwang ES: Modulation of mitochondrial membrane potential and ROS generation by nicotinamide in a manner independent of SIRT1 and mitophagy. Mol Cells 40: 503-514, 2017.
27. Peixoto P, Grandvallet C, Feugeas JP, Guittaut M and Hervouet E: Epigenetic control of autophagy in cancer cells: A key process for cancer-related phenotypes. Cells 8: 1656, 2019.
28. Zachari M and Ktistakis NT: Mammalian mitophagosome formation: A focus on the early signals and steps. Front Cell Dev Biol 8: 171, 2020.
29. Walsh BK, Brooks TM and Grenier BM: Oxygen therapy in the neonatal care environment. Respir Care 54: 1193-1202, 2009.
30. Jobe AH and Kallapur SG: Long term consequences of oxygen therapy in the neonatal period. Semin Fetal Neonatal Med 15: 230-235, 2010.
31. Wang J and Dong W: Oxidative stress and bronchopulmonary dysplasia. Gene 678: 177-183, 2018.
32. Bancalari E, Claure N and Sosenko IR: Bronchopulmonary dysplasia: Changes in pathogenesis, epidemiology and definition. Semin Neonatol 8: 63-71, 2003.
33. Scherz-Shouval R and Elazar Z: Regulation of autophagy by ROS: Physiology and pathology. Trends Biochem Sci 36: 30-38, 2011.
34. El-Merhie N, Baumgart-Vogt E, Pilatz A, Pfreimer S, Pfeiffer B, Pak O, Kosanovic D, Seimetz M, Schermuly RT, Weissmann N and Karnati S: Differential alterations of the mitochondrial morphology and respiratory chain complexes during postnatal development of the mouse lung. Oxid Med Cell Longev 2017: 9169146, 2017.
35. Anzell AR, Maizy R, Przyklenk K and Sanderson TH: Mitochondrial quality control and disease: Insights into ischemia-reperfusion injury. Mol Neurobiol 55: 2547-2564, 2018.
36. Eiyama A and Okamoto K: PINK1/Parkin-mediated mitophagy in mammalian cells. Curr Opin Cell Biol 33: 95-101, 2015.
37. Ahmad T, Sundar IK, Lerner CA, Gerloff J, Tormos AM, Yao H and Rahman I: Impaired mitophagy leads to cigarette smoke stress-induced cellular senescence: Implications for chronic obstructive pulmonary disease. FASEB J 29: 2912-2929, 2015.
38. Patel AS, Song JW, Chu SG, Mizumura K, Osorio JC, Shi Y, El-Chemaly S, Lee CG, Rosas IO, Elias JA, *et al*: Epithelial cell mitochondrial dysfunction and PINK1 are induced by transforming growth factor-beta1 in pulmonary fibrosis. PLoS One 10: e0121246, 2015.
39. Araya J, Tsubouchi K, Sato N, Ito S, Minagawa S, Hara H, Hosaka Y, Ichikawa A, Saito N, Kadota T, *et al*: PRKN-regulated mitophagy and cellular senescence during COPD pathogenesis. Autophagy 15: 510-526, 2019.
40. Zhang D, Wu L, Du Y, Zhu Y, Pan B, Xue X and Fu J: Autophagy inducers restore impaired autophagy, reduce apoptosis, and attenuate blunted alveolarization in hyperoxia-exposed newborn rats. Pediatr Pulmonol 53: 1053-1066, 2018.
41. Durcan TM and Fon EA: The three 'P's of mitophagy: PARKIN, PINK1, and post-translational modifications. Genes Dev 29: 989-999, 2015.
42. Esteban-Martinez L, Sierra-Filardi E, McGreal RS, Salazar-Roa M, Mariño G, Seco E, Durand S, Enot D, Graña O, Malumbres M, *et al*: Programmed mitophagy is essential for the glycolytic switch during cell differentiation. EMBO J 36: 1688-1706, 2017.
43. Esteban-Martinez L and Boya P: BNIP3L/NIX-dependent mitophagy regulates cell differentiation via metabolic reprogramming. Autophagy 14: 915-917, 2018.
44. Gao F, Chen D, Si J, Hu Q, Qin Z, Fang M and Wang G: The mitochondrial protein BNIP3L is the substrate of PARK2 and mediates mitophagy in PINK1/PARK2 pathway. Hum Mol Genet 24: 2528-2538, 2015.
45. Zhao H, Dennery PA and Yao H: Metabolic reprogramming in the pathogenesis of chronic lung diseases, including BPD, COPD, and pulmonary fibrosis. Am J Physiol Lung Cell Mol Physiol 314: L544-L554, 2018.
46. Lottes RG, Newton DA, Spyropoulos DD and Baatz JE: Lactate as substrate for mitochondrial respiration in alveolar epithelial type II cells. Am J Physiol Lung Cell Mol Physiol 308: L953-L961, 2015.
47. Ratner V, Starkov A, Matsiukevich D, Polin RA and Ten VS: Mitochondrial dysfunction contributes to alveolar developmental arrest in hyperoxia-exposed mice. Am J Respir Cell Mol Biol 40: 511-518, 2009.
48. Das KC: Hyperoxia decreases glycolytic capacity, glycolytic reserve and oxidative phosphorylation in MLE-12 cells and inhibits complex I and II function, but not complex IV in isolated mouse lung mitochondria. PLoS One 8: e73358, 2013.
49. Simon LM, Raffin TA, Douglas WH, Theodore J and Robin ED: Effects of high oxygen exposure on bioenergetics in isolated type II pneumocytes. J Appl Physiol Respir Environ Exerc Physiol 47: 98-103, 1979.
50. Naik PP, Birbrair A and Bhutia SK: Mitophagy-driven metabolic switch reprograms stem cell fate. Cell Mol Life Sci 76: 27-43, 2019.
51. McCoy MK, Kaganovich A, Rudenko IN, Ding J and Cookson MR: Hexokinase activity is required for recruitment of parkin to depolarized mitochondria. Hum Mol Genet 23: 145-156, 2014.
52. Liu K, Li F, Han H, Chen Y, Mao Z, Luo J, Zhao Y, Zheng B, Gu W and Zhao W: Parkin regulates the activity of pyruvate kinase M2. J Biol Chem 291: 10307-10317, 2016.